Polymorphism in Bismuth Stannate: A First-Principles Study

Aron Walsh*,† and Graeme W. Watson*

School of Chemistry, Trinity College, University of Dublin, Dublin 2, Ireland

Received May 25, 2007. Revised Manuscript Received August 7, 2007

From the wide range of Sn^{IV}-based pyrochlores, $Bi_2Sn_2O_7$ stands out as a material that deviates from the standard cubic-lattice symmetry. At low temperatures, $Bi_2Sn_2O_7$ adopts a distorted monoclinic $\sqrt{2} \times \sqrt{2} \times 2$ expansion of the pyrochlore structure (α-phase) and only favors the cubic lattice (γ-phase) above 900 K. In this study, we calculate and examine the electronic structure of both the α- and γ-phases of $Bi_2Sn_2O_7$ and compare them to the results of two regular pyrochlore materials, $La_2Sn_2O_7$ and $Y_2Sn_2O_7$. Our analysis highlights the importance of covalent interactions between the electronic states of the metal with O 2p in $Bi_2Sn_2O_7$, which are not present in the other oxides. The formation of an asymmetric electron density on Bi is observed as the driving force behind the distorted geometry favored by $Bi_2Sn_2O_7$.

Introduction

Ternary oxides of the form $A_2M_2O_7$ generally adopt the cubic pyrochlore structure and have long been a matter of interest due to their substantial range of properties such as ionic conduction,[1] ferromagnetism,[2] superconduction,[3] and high dielectric character.[4,5] In addition, these materials display a number of important catalytic and gas-sensing properties.[6−10] Of particular interest have been the Sn-based pyrochlores such as $Bi_2Sn_2O_7$, due to their catalytic activity in a number of important processes including the oxidation of hydrocarbons and the partial oxidation of isobutene.[8] In terms of gas sensing, they have exhibited strong selectivity toward CO.[9] Other Sn pyrochlores that have gathered recent interest include $La_2Sn_2O_7$, which exhibits activity in the decomposition of NO_x,[10] and $Y_2Sn_2O_7$, which displays strong photocatalytic properties.[11]

The majority of $A_2Sn_2O_7$ metal stannates favor the cubic pyrochlore structure with space group *Fd*3*m* and contain eight formula units per unit cell, as shown in Figure 1a. The A ions (generally in a low II/III oxidation state) are surrounded by eight oxygens in a distorted cubic polyhedron, with the Sn^{IV} ions coordinated by six oxygens in an octahedron. A comprehensive structural examination of Sn pyrochlores with A = Y, La, Pr, Nd, Tb, Dy, Ho, Er, Tm, Yb, and Lu has been performed by Kennedy et al.[12] using X-ray powder diffraction. Bond valence sum calculations on their structural data indicate the presence of at least some covalent interactions in these compounds.

$Bi_2Sn_2O_7$ is unique among metal stannates as it does not adopt the cubic pyrochlore structure as its thermodynamically stable phase, instead existing in a number of polymorphs.[13,14] The thermodynamically stable phase, α-$Bi_2Sn_2O_7$, is a monoclinic ($\beta = 90.04°$) $\sqrt{2} \times \sqrt{2} \times 2$ expansion of the regular cubic pyrochlore lattice, and its crystal structure has only been recently determined through a combination of diffraction data and simulated annealing by Evans et al. .[15] It is one of the most complex oxide structures to have been solved by powder diffraction (32 formula units per cell, Figure 1b). Here, the Bi atoms are distorted from their ideal pyrochlore positions. At 130 °C, face-centered cubic β-$Bi_2Sn_2O_7$ becomes favored until above 630 °C, where the cubic pyrochlore-based γ-phase is finally adopted.

Low-symmetry crystal structures in group 14 and 15 metal oxides are commonly associated with the existence of a lower metal oxidation state (Sn^{II}, Pb^{II}, Bi^{III}) and the formation of a stereochemically active ns^2 lone electron pair.[16] In $Bi_2Sn_2O_7$, Sn is considered to adopt its upper oxidation state of IV ($4d^{10}5s^05p^0$), while an oxidation state of III is ascribed

* To whom correspondence should be addressed. E-mail: aron_walsh@nrel.gov (A.W.), watsong@tcd.ie (G.W.W.).

† Present address: National Renewable Energy Laboratory, Golden, Colorado 80401.

(1) Abrantes, J. C. C.; Levchenko, A.; Shlyakhtina, A. V.; Shcherbakova, L. G.; Horovistiz, A. L.; Fagg, D. P.; Frade, J. R. *Solid State Ionics* **2006**, *177*, 1785.
(2) Booth, C. H.; Gardner, J. S.; Kwei, G. H.; Heffner, R. H.; Bridges, F.; Subramanian, M. A. *Phys. Rev. B: Condens. Matter Mater. Phys.* **2000**, *62*, R755.
(3) Manalo, S.; Michor, H.; Hilscher, G.; Bruhwiler, M.; Batlogg, B. *Phys. Rev. B: Condens. Matter Mater. Phys.* **2006**, *73*.
(4) Du, H. L.; Yao, X.; Wang, H. *Appl. Phys. Lett.* **2006**, *88*.
(5) Melot, B.; Rodriguez, E.; Proffen, T.; Hayward, M. A.; Seshadri, R. *Mater. Res. Bull.* **2006**, *41*, 961.
(6) Jorissen, L. *J. Power Sources* **2006**, *155*, 23.
(7) Ke, J. H.; Kumar, A. S.; Sue, J. W.; Venkatesan, S.; Zen, J. M. *J. Mol. Catal. A*: *Chem.* **2005**, *233*, 111.
(8) Moens, L.; Ruiz, P.; Delmon, B.; Devillers, M. *Appl. Catal., A* **1999**, *180*, 299.
(9) Coles, G. S. V.; Bond, S. E.; Williams, G. *J. Mater. Chem.* **1994**, *4*, 23.
(10) Park, S.; Song, H. S.; Choi, H.-J.; Moon, J. *Solid State Ionics* **2004**, *175*, 625.
(11) Wang, S. M.; Zhou, G. J.; Lu, M. K.; Zhou, Y. Y.; Sen, Yang, Z. *J. Alloys Compd.* **2006**, *424*, L3.
(12) Kennedy, B. J.; Hunter, B. A.; Howard, C. J. *J. Solid State Chem.* **1997**, *130*, 58.
(13) Kennedy, I.; Kennedy, B. J.; Hunter, B. A.; Vogt, T. *J. Solid State Chem.* **1997**, *131*, 317.
(14) Kennedy, B. J.; Ismunandar; Elcombe, M. M. In *EPDIC 5, Proc. Eur. Powder Diff. Conf. 5th, 1997, Part 1−2*; *Mater. Sci. Forum* **1998**, *278−282*, 762.
(15) Evans, I. R.; Howard, J. A. K.; Evans, J. S. O. *J. Mater. Chem.* **2003**, *13*, 2098.
(16) Orgel, L. E. *J. Chem. Soc.* **1959**, *1959*, 3815.

10.1021/cm0714279 CCC: $37.00
Published on Web 09/27/2007

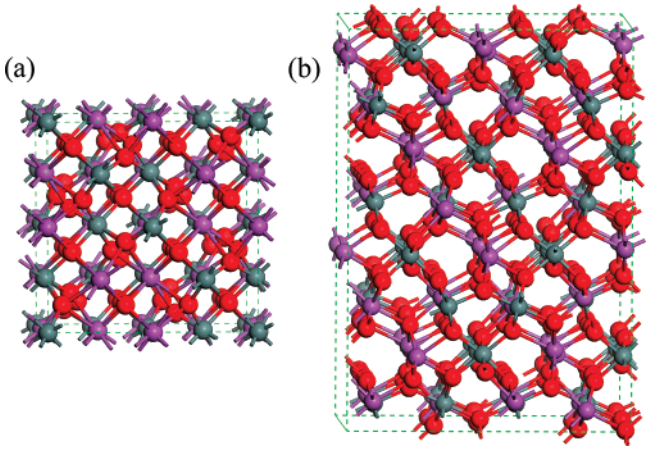

Figure 1. (a) Cubic pyrochlore crystal structure of γ-$Bi_2Sn_2O_7$. (b) The monoclinic crystal structure of α-$Bi_2Sn_2O_7$, with 32 formula units per cell. The O atoms are in red, the Sn atoms are in gray, and the Bi atoms are in purple.

to Bi ($5d^{10}6s^26p^0$). The presence of the Bi lone-pair $6s^2$ electrons has been suggested as being important in the catalytic oxidation processes of $Bi_2Sn_2O_7$.[14] We have performed a series of theoretical and experimental studies investigating the origins of electronic and structural distortions in post-transition metal oxides[17−26] that indicate that these cation lone pairs do not conform to the classical ns^2 lone-pair model.[16] The anion plays an important role in bridging the gap between the cation s and p states, which are too far apart in energy to couple directly. In the binary metal oxides, the interaction of O 2p with cation s character results in a filled antibonding combination at the top of the valence band. This produces the high-energy cation s states required for effective coupling with the cation p state, as shown schematically in Figure 2. It is these states at the *top* of the valence band that are responsible for the asymmetry in the electron density of the cation. This model has recently been shown to apply in BiB_3O_6 on the basis of hybrid density functional theory (DFT) calculations.[27] As such, the role of the Bi 6s electrons in $Bi_2Sn_2O_7$ will be more complicated than classical intra-atomic "inert electron pair" hybridization considerations would suggest and may have an interesting role to play in surface catalytic and gas-sensing processes.

Experimentally, a number of structural studies of $Bi_2Sn_2O_7$ have been performed,[13−15,28−30] and there has also been in-depth investigation of its catalytic activity.[8] We recently reported a combined X-ray photoemission spectroscopy and DFT study of the α-phase of $Bi_2Sn_2O_7$ in which our calculated electronic properties were in very good agreement with the experimental spectra.[24] Due to the computational restrictions imposed by the large unit cell, no other calculations on α-$Bi_2Sn_2O_7$ have been reported at this time. Theoretical studies of the regular pyrochlore materials are more abundant.[31−36] The most comprehensive study, performed by Prundeda and Artacho,[31] systematically examined the elastic and electronic properties of a wide range of La- and Y-based pyrochlores using DFT within the local density approximation. The results indicated an increase in ionicity of these pyrochlores on changing the B cation from Sn → Ti → Hf → Zr.

In this paper, we report a detailed examination of the first-principles electronic structure of both α-$Bi_2Sn_2O_7$ and γ-$Bi_2Sn_2O_7$ with a view to understanding the polymorphism and structural deviance exhibited by $Bi_2Sn_2O_7$. For comparison, the electronic structure of the regular pyrochlores $La_2Sn_2O_7$ and $Y_2Sn_2O_7$ is also presented. Investigations of the electronic density of states (EDOS), valence-electron density, and partial charges are used to shed light on the underlying interactions in these materials. The formation of a weak asymmetric electron density (lone pair) on Bi is found to be the driving force behind the distorted geometry favored by $Bi_2Sn_2O_7$. The competition between the upper and lower oxidation states of Bi, Pb, and Sn is also discussed.

Methods

DFT[37,38] as embodied in the *Vienna Ab Initio Simulation Package*[39,40] was used to calculate the electronic structures of the α- and γ-phases of $Bi_2Sn_2O_7$ and the thermodynamically stable cubic pyrochlore phase of both $La_2Sn_2O_7$ and $Y_2Sn_2O_7$. In each case, the atomic positions were fully relaxed until the forces had converged to less than 0.005 eV/Å and the pressure on the cell had equalized (constant volume). A gradient-corrected exchange-correlation functional was employed using the derivation of Perdew et al.[41]

Three-dimensional periodic boundary conditions were applied to approximate a bulk solid, with the wavefunctions represented in

(17) Payne, D. J.; Egdell, R. G.; Walsh, A.; Watson, G. W.; Guo, J.; Glans, P. A.; Learmonth, T.; Smith, K. E. *Phys. Rev. Lett.* **2006**, *96*, 157403.
(18) Walsh, A.; Watson, G. W.; Payne, D. J.; Edgell, R. G.; Guo, J. H.; Glans, P. A.; Learmonth, T.; Smith, K. E. *Phys. Rev. B: Condens. Matter Mater. Phys.* **2006**, *73*, 235104.
(19) Walsh, A.; Watson, G. W. *Phys. Rev. B: Condens. Matter Mater. Phys.* **2004**, *70*, 235114.
(20) Glans, P. A.; Learmonth, T.; Smith, K. E.; Guo, J.; Walsh, A.; Watson, G. W.; Terzi, F.; Egdell, R. G. *Phys. Rev. B: Condens. Matter Mater. Phys.* **2005**, *71*, 235109.
(21) Walsh, A.; Watson, G. W. *J. Phys. Chem. B* **2005**, *109*, 18868.
(22) Glans, P. A.; Learmonth, T.; McGuinness, C.; Smith, K. E.; Guo, J. H.; Walsh, A.; Watson, G. W.; Egdell, R. G. *Chem. Phys. Lett.* **2004**, *399*, 98.
(23) Walsh, A.; Watson, G. W. *J. Solid State Chem.* **2005**, *178*, 1422.
(24) Walsh, A.; Watson, G. W.; Payne, D. J.; Atkinson, G.; Egdell, R. G. *J. Mater. Chem.* **2006**, *16*, 3452.
(25) Watson, G. W. *J. Chem. Phys.* **2001**, *114*, 758.
(26) Watson, G. W.; Parker, S. C.; Kresse, G. *Phys. Rev. B: Condens. Matter Mater. Phys.* **1999**, *59*, 8481.
(27) Yang, J.; Dolg, M. *Phys. Chem. Chem. Phys.* **2007**, *9*, 2094.
(28) Shannon, R. D.; Bierlein, J. D.; Gillson, J. L.; Jones, G. A.; Sleight, A. W. *J. Phys. Chem. Solids* **1980**, *41*, 117.
(29) Vetter, G.; Queyroux, F.; Gilles, J. C. *Mater. Res. Bull.* **1978**, *13*, 211.
(30) Kahlenberg, V.; Zeiske, T. *Z. Kristallogr.* **1997**, *212*, 297.
(31) Pruneda, J. M.; Artacho, E. *Phys. Rev. B: Condens. Matter Mater. Phys.* **2005**, *72*, *085107*.
(32) Terki, R.; Bertrand, G.; Aourag, H.; Coddet, C. *Physica B* **2007**, *392*, 341.
(33) Saha-Dasgupta, T.; de Raychaudhury, M.; Sarma, D. D. *Phys. Rev. Lett.* **2006**, *96*, 087205.
(34) Crocombette, J. P.; Chartier, A. *Nucl. Instrum. Methods Phys. Res., Sect. B* **2007**, *255*, 158.
(35) Wilde, P. J.; Catlow, C. R. A. *Solid State Ionics* **1998**, *112*, 173.
(36) Todorov, I. T.; Allan, N. L.; Purton, J. A.; Dove, M. T.; Smith, W. *J. Mater. Sci.* **2007**, *42*, 1920.
(37) Hohenberg, P.; Kohn, W. *Phys. Rev.* **1964**, *136*, B864.
(38) Kohn, W.; Sham, L. J. *Phys. Rev.* **1965**, *140*, A1133.
(39) Kresse, G.; Furthmüller, J. *Comput. Mater. Sci.* **1996**, *6*, 15.
(40) Kresse, G.; Furthmüller, J. *Phys. Rev. B: Condens. Matter Mater. Phys.* **1996**, *54*, 11169.
(41) Perdew, J. P.; Burke, K.; Ernzerhof, M. *Phys. Rev. Lett.* **1996**, *77*, 3865.

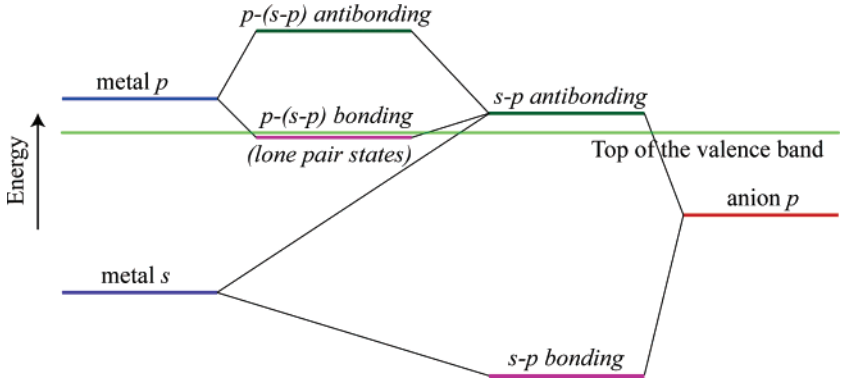

Figure 2. Schematic energy level diagram of the interactions observed in the binary Pb, Sn, and Bi oxides, which lead to the formation of an asymmetric electron density (lone pair) on the cation.

Table 1. Calculated Binding Energies (per $A_2B_2O_7$ Formula Unit) and Structural Data for the α- and γ-Phases of $Bi_2Sn_2O_7$ and Pyrochlore-Structured $La_2Sn_2O_7$ and $Y_2Sn_2O_7$[a]

	material			
	α-$Bi_2Sn_2O_7$	γ-$Bi_2Sn_2O_7$	$La_2Sn_2O_7$	$Y_2Sn_2O_7$
binding energy (eV)	−4.87	−4.67	−5.67	−5.05
V (Å^3)	5118.46	1244.86	1244.79	1164.37
a (Å)	15.34 (+1.9%)	10.76 (+0.1%)	10.76 (+0.6%)	10.52 (+1.5%)
c (Å)	21.74 (+1.1%)			
β (deg)	90.04			

[a] Percentage error is given with respect to experimental data.

terms of a plane-wave basis set. The projector-augmented wave method[42] was used to represent the interaction between the core electrons (Sn: [Kr], Bi: [Xe], La: [Pd], Y: [Ni], O: [He]) and the valence electrons, as it offers good precision while maintaining the computational efficiency of the traditional pseudopotential approach. The fixed core states were generated from all-electron relativistic calculations. Convergence of the plane-wave cutoff and k-point grid density to 0.01 eV/formula unit resulted in a 500 eV plane-wave cutoff. A Monkhorst−Pack[43] special k-point grid of 3 × 3 × 3 was employed for α-$Bi_2Sn_2O_7$, resulting in a total number of 14 irreducible k-points, while a 6 × 6 × 6 grid was used for the regular pyrochlore structures, resulting in 36 irreducible k-points to map the first Brillouin zone.

Results

Equilibrium Structures. Structural optimization of each material at a series of finite volumes was performed, allowing the atomic positions, the lattice vectors, and cell angles to relax within a volume-constrained cell. The resulting energy−volume data were fitted to the Murnaghan equation of state[44] to obtain the equilibrium cell volumes. This approach is taken to avoid the problem of the Pulay stress and changes in the effective basis set and its cutoff that occur in plane-wave calculations on volume changes. The optimized cell parameters are listed in Table 1. The binding energies were calculated relative to the DFT total energies of the stable binary oxides of the cation constituents, i.e., SnO_2, Bi_2O_3, Y_2O_3, and La_2O_3.

For α-$Bi_2Sn_2O_7$, the equilibrium structure preserved the slight monoclinic distortion of the unit cell ($\beta = 90.04$), with the calculated lattice vectors within 2% of the experimentally determined values.[15] Each Bi atom is five-coordinate with respect to oxygen, with the Bi−O nearest-neighbor distances ranging from 2.25 to 2.50 Å. These are comparable to the stable phase of Bi_2O_3 where the five Bi−O nearest-neighbor distances range from 2.19 to 2.59 Å.[18] The geometry around a single Bi atom is shown in Figure 3a. The Sn atoms are six-coordinate with respect to oxygen and have Sn−O nearest-neighbor distances ranging from 2.04 to 2.15 Å. The coordination symmetry around Sn is lower than that of octahedral rutile SnO_2, with three pairs of matching Sn−O bond lengths found, as shown for a single Sn atom in Figure 3b. Both the Bi and Sn coordination data are in good agreement with the reported X-ray diffraction studies.[15]

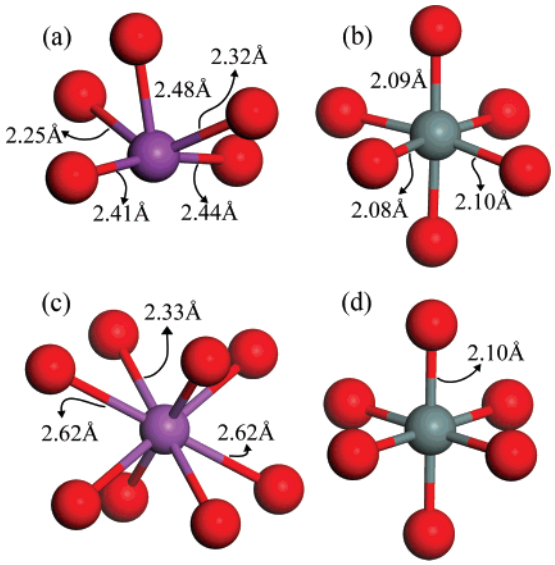

Figure 3. Coordination environment around (a) a Bi atom and (b) a Sn atom in α-$Bi_2Sn_2O_7$ and (c) a Bi atom and (d) a Sn atom in γ-$Bi_2Sn_2O_7$.

The lattice vector of the relaxed γ-$Bi_2Sn_2O_7$ unit cell (10.76 Å) is in excellent agreement with the experimental structure[30] (within 1%). While optimization does result in a local minimum, the calculated binding energy, relative to Bi_2O_3 and SnO_2, is 0.2 eV/formula unit less stable than that of α-$Bi_2Sn_2O_7$, as would be expected for a high-temperature phase. The interatomic distances in γ-$Bi_2Sn_2O_7$ reflect the higher-symmetry crystal structure. Here, the Bi sites are eight-coordinate with respect to oxygen (2 × 2.33 and 6 × 2.62 Å; Figure 3c). The Sn sites are again six-coordinate;

(42) Kresse, G.; Joubert, D. *Phys. Rev. B: Condens. Matter Mater. Phys.* **1999**, *59*, 1758.
(43) Monkhorst, H. J.; Pack, J. D. *Phys. Rev. B* **1976**, *13*, 5188.
(44) Murnaghan, F. D. *Proc. Natl. Acad. Sci. U.S.A.* **1944**, *30*, 244.

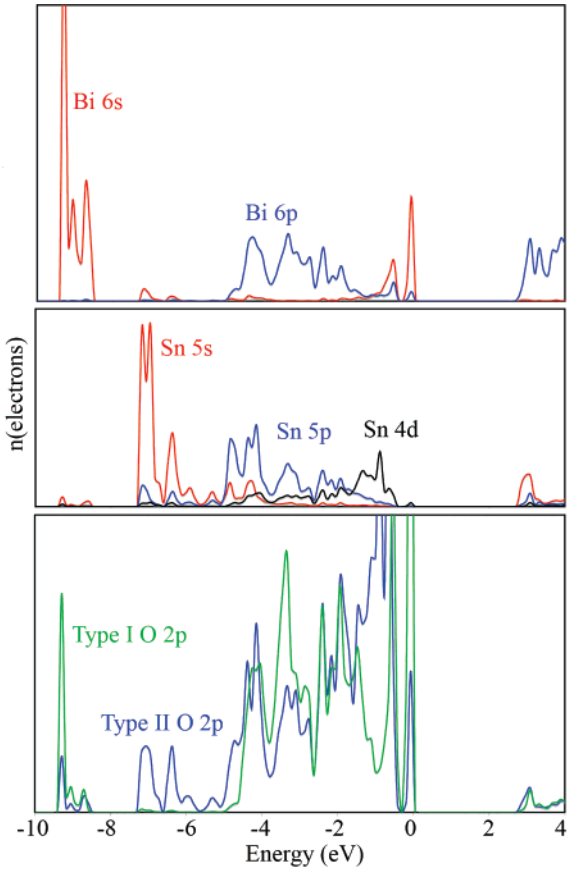

Figure 4. Partial EDOS of α-$Bi_2Sn_2O_7$, plotted with reference to the top of the valence band.

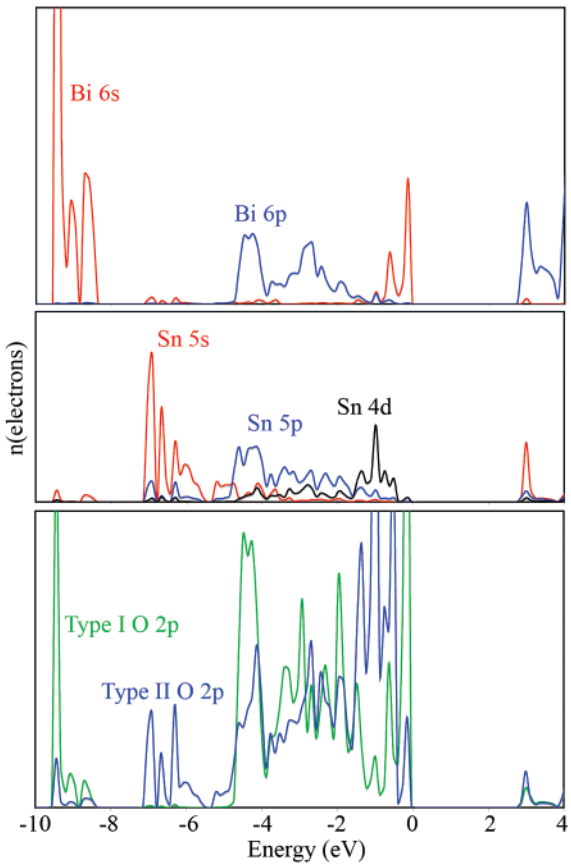

Figure 5. Partial EDOS of γ-$Bi_2Sn_2O_7$, plotted with reference to the top of the valence band.

however, in this case, octahedral symmetry is found (6 × 2.10 Å; Figure 3d).

Optimization of $La_2Sn_2O_7$ in the cubic pyrochlore structure results in the same optimized lattice vector as that in γ-$Bi_2Sn_2O_7$ (as would be expected for a cation of similar size), which is within 1% of the experimental value.[12] The equilibrium lattice vector for $Y_2Sn_2O_7$ is smaller (10.52 Å) due to the reduced ionic radius of Y and is within 2% of the experimental value. Both materials show the same coordination features and symmetry exhibited by γ-$Bi_2Sn_2O_7$. For $Y_2Sn_2O_7$, the Sn−O interatomic distance is reduced to 2.08 Å.

Electronic Density of States. The partial electronic DOS (PEDOS) for each material are shown in Figures 4−7. The plots are made from −10 to 4 eV with reference to the top of the valence band at 0 eV. As a plane-wave basis set was employed, to calculate these *l* and *m* decomposed EDOS, the wavefunctions were projected onto spherical harmonics centered on each lattice site. Various radii were tested to ensure agreement with charge density plots, reasonable space filling, and that integration resulted in the correct number of electrons. The results (at least the qualitative aspects) are insensitive to a change in the radii (1.55 Å for Bi and La, 1.50 Å for Sn and Y, and 1.45 Å for O).

While the band structures along the high-symmetry lines were not calculated, the large unit cells involved would be expected to result in minimal band dispersions away from the zone center, and hence, the calculated direct band gaps at the Γ point of 2.65 eV (α-$Bi_2Sn_2O_7$), 2.74 eV (γ-$Bi_2Sn_2O_7$), 2.89 eV ($La_2Sn_2O_7$), and 2.83 eV ($Y_2Sn_2O_7$) are a reasonable approximation. Unfortunately, we are not aware of any experimental band-gap measurements or optical studies of these materials. However, nanorods of $La_2Sn_2O_7$ have been reported to undergo emission at a wavelength of

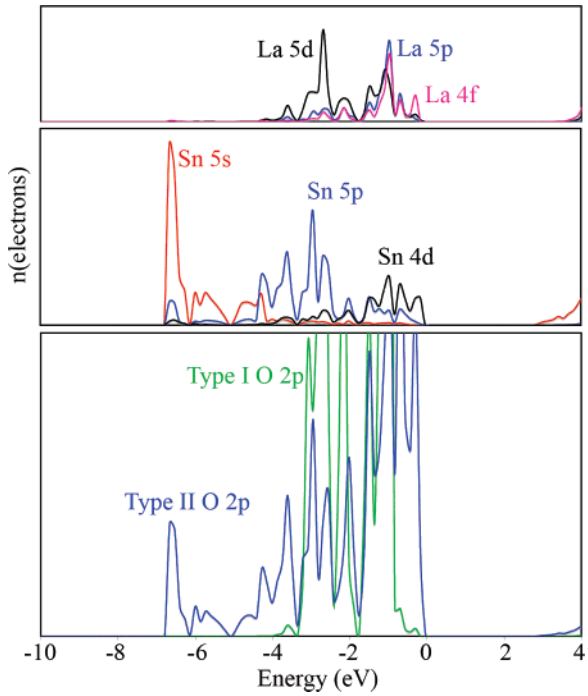

Figure 6. Partial EDOS of $La_2Sn_2O_7$, plotted with reference to the top of the valence band.

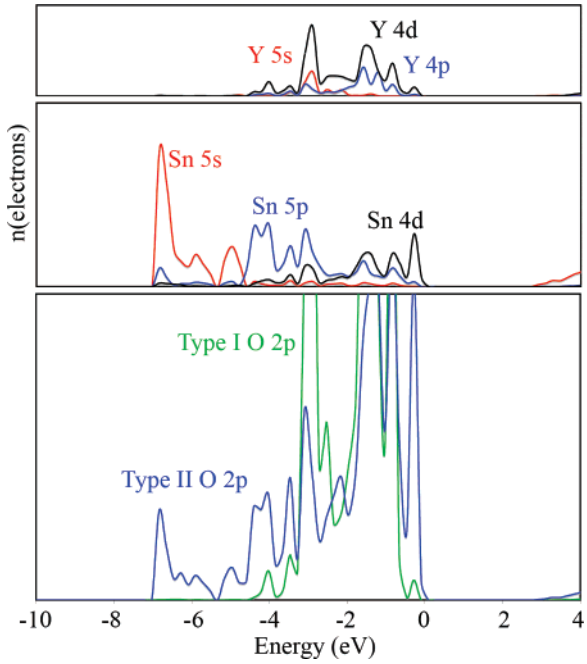

Figure 7. Partial EDOS of $Y_2Sn_2O_7$, plotted with reference to the top of the valence band.

400 nm, which would suggest a band gap in the region of 2.95 eV.[11]

For α-$Bi_2Sn_2O_7$, the valence band runs from −10 to 0 eV, with the onset of the conduction band at +2.5 eV (Figure 4). The Bi 6s contribution to the EDOS is split between the top and bottom of the valence band, with the majority of states situated in the latter. A substantial Bi 6p contribution is present from −6 to 0 eV. The presence of the high-energy Bi 6s states at the top of the valence band is consistent with the interactions observed in the binary Bi_2O_3 oxide.[27] The bottom of the conduction band is dominated by Bi 6p states. The Sn 5s contribution to the DOS is split between the valence and conduction bands. In the valence band, the Sn 5s states are spread between −7 and −4 eV. A peak consisting of Sn 5p states runs from −5 to 0 eV. A small contribution from Sn 4d is also found at the top of the valence band.

The two types of oxygen coordination site present in α-$Bi_2Sn_2O_7$ result in two unique oxygen PEDOS. The first oxygen site (labeled type I) has tetrahedral coordination to four Bi atoms. The second site (type II) is straddled between two Sn atoms and a single Bi atom. These coordination features are mirrored in the PEDOS. For type I oxygen, there is a strong overlap of O 2p with the Bi 6s peak at the bottom of the valence band. O 2p states are present between −5 and −2 eV overlapping with Bi 6p. An additional peak is found at the top of the valence band overlapping with the high-energy Bi 6s states. The PEDOS derived for type II oxygen shows more overlap with the Sn states, as expected. The peak at −10 eV is diminished, with O 2p derived states now present between −9 and −6 eV overlapping with Sn 5s. The O 2p peak at the top of the valence band is also reduced.

The PEDOS of γ-$Bi_2Sn_2O_7$ (Figure 5) retains many of the features observed for α-$Bi_2Sn_2O_7$. The Bi 6s states are again split between the top and bottom of the valence band. The most notable change in the distribution of the Bi 6p states is

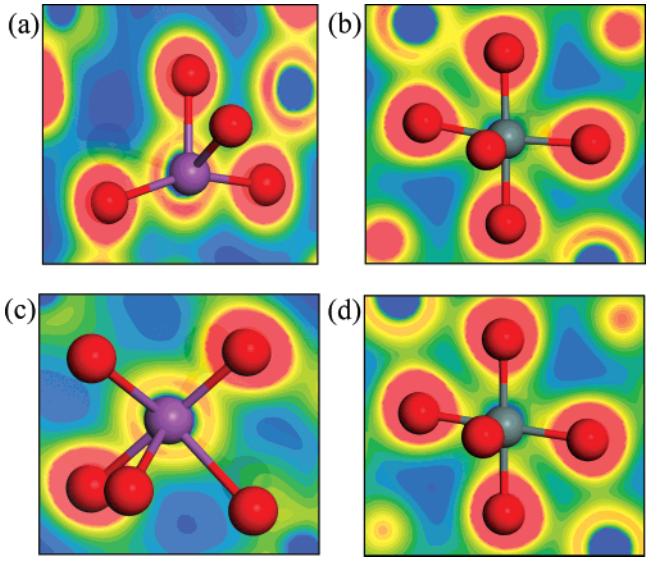

Figure 8. Valence-electron density contour maps around (a) Bi and (b) Sn in α-$Bi_2Sn_2O_7$ and (c) Bi and (d) Sn in γ-$Bi_2Sn_2O_7$. The contours are shown from blue (0 e·Å^{-3}) to red (0.5 e·Å^{-3}).

the reduction at the top of the valence band, between −1 and 0 eV. The placement of the Sn 5s, 5p, and 4d states is largely unchanged from that of α-$Bi_2Sn_2O_7$. Two types of oxygen site are present, with the distribution of electronic states again mirroring their respective coordination environments. Here, the type I oxygen again has tetrahedral coordination to four Bi ions, while the type II oxygen is now bridged between two Sn ions.

The PEDOS resulting from $La_2Sn_2O_7$ and $Y_2Sn_2O_7$ are shown in Figures 6 and 7. The distribution of the Sn 5s and 5p states is qualitatively similar to both phases of $Bi_2Sn_2O_7$. However, there is a substantial difference in the PEDOS derived from the pyrochlore A cations. For $La_2Sn_2O_7$ and $Y_2Sn_2O_7$, the contribution of the La/Y states to the valence band is confined between −4 and 0 eV. No La/Y contributions are found at the bottom of the valence band. The La valence band is dominated by La 5d, with smaller contributions from p- and f-derived states, while the Y valence band is a mixture of Y 5s, 4d, and 4p. The PEDOS of type I oxygen (coordinated to the A metal) is now localized between −4 and −1 eV. There is no overlap with the metal s states (as observed for Bi). As such, there are no O 2p states observed at low energies, and there is no separated high-energy O 2p peak at the top of the valence band overlapping with the metal A states. The PEDOS of the Sn-coordinated type II oxygen remains largely unchanged as expected.

Valence-Electron Density. The valence-electron density has been calculated from −10 to 0 eV to remove higher-binding-energy states (Sn 4d and Bi 5d) that do not contribute significantly to the chemical bonding. Contour slices through Bi and Sn atoms in both α- and γ-$Bi_2Sn_2O_7$ are shown in Figure 8. The electron density around the O atoms is approximately spherical in each case. The electronic distribution around the Bi atoms in α-$Bi_2Sn_2O_7$ is distorted, pointing away from the five-coordinated O atoms (Figure 8a). This is evidence of a weakly directional Bi asymmetric electron density (lone pair). The lost coordination of an oxygen is

Table 2. Partial Charges for the α- and γ-Phases of $Bi_2Sn_2O_7$ and Pyrochlore-Structured $La_2Sn_2O_7$ and $Y_2Sn_2O_7$ Calculated from Bader Analysis

partial charge	α-$Bi_2Sn_2O_7$	γ-$Bi_2Sn_2O_7$	$La_2Sn_2O_7$	$Y_2Sn_2O_7$
Sn	+2.5	+2.4	+2.4	+2.4
Bi/La/Y	+1.9	+2.0	+2.1	+2.2
O	−1.2/−1.3	−1.3	−1.3/−1.4	−1.3/−1.4

compensated by an enhanced electron density in its place. In γ-$Bi_2Sn_2O_7$, this is not the case (Figure 8c). The symmetric coordination environment produces a more evenly distributed electron density around the Bi atoms. For Sn, the similar coordination sites result in an almost identical electron distribution around the atoms for both phases (Figure 8b,d). The electron density around the Sn atoms is much weaker compared with that of Bi, which is in line with its higher oxidation state.

Partial Charges. As a nonlocal plane-wave basis set is employed in our calculations, the assignment of accurate partial charges is a nontrivial matter. The most straightforward method of assigning a quantitative charge to the atomic centers is through rigid sphere partitioning at fixed radii; however, this may lead to inaccuracies due to the asymmetric nature of the charge density in distorted structures and excessive overlap between adjacent spheres. An improvement is offered through partitioning of the charge density following the work of Bader,[45] which analyses the natural contours in the equilibrium electron density to assign the electronic charges to each lattice site. This method, as implemented by Henkelman et al.,[46] has been utilized in our analysis.

The calculated partial charges from the converged electron density for each of the four materials studied are listed in Table 2. For Sn, the charge of approximately +2.5 is clearly less than the oxidation state of IV traditionally assigned to Sn but is in line with both the EDOS, which shows occupation of approximately half the Sn 5s states, and the calculated partial charge of Sn in bulk SnO_2.[47] There is a difference of +0.1 from the charge of Sn in the distorted α-phase and the remaining cubic pyrochlore structures. The partial charge of the A cation increases sequentially from +1.9 for Bi in α-$Bi_2Sn_2O_7$ to +2.2 for Y in $Y_2Sn_2O_7$. There is a corresponding decrease in the O partial charges from −1.2 to −1.4.

Discussion

Analysis of the electronic structure of the α- and γ-phases of $Bi_2Sn_2O_7$ indicates that the same fundamental interactions occur in each material. There is a high degree of covalency as demonstrated by the overlap between the metal s and p and O 2p states. For Bi, the calculated PEDOS is consistent with our previous analysis of Bi_2O_3 where there is a bonding Bi 6s/O 2p combination with majority Bi 6s character at the bottom of the valence band and a corresponding filled antibonding Bi 6s/O 2p combination with majority O 2p at the top of the valence band. For Sn, there is also a bonding Sn 5s/O 2p interaction present at the bottom of the valence band; however, the corresponding antibonding combination is unfilled at the bottom of the conduction band. In this way, the band gaps in α- and γ-$Bi_2Sn_2O_7$ are determined by hybridized Bi/O states at the top of the valence band and hybridized Sn/O states at the bottom of the conduction band. Differences in the detailed electronic structure of the two phases of $Bi_2Sn_2O_7$ come in the coupling of Bi 6p states with high-energy O 2p and Bi 6s states at the top of the valence band. For α-$Bi_2Sn_2O_7$, this coupling leads to the formation of an asymmetric electronic density on Bi, which can compensate for the lost oxygen coordination in the distorted structure. For γ-$Bi_2Sn_2O_7$, the symmetric coordination environment inhibits the coupling of Bi 6p at the top of the valence band and hence is less favored energetically as the antibonding states at the top of the valence band cannot be stabilized. The preference of $Bi_2Sn_2O_7$ for a distorted structure is therefore directly related to the formation of the Bi lone pair. The PEDOS show that the interaction of O 2p with the valence states of Y and La is limited in comparison to Bi and no antibonding states are produced at the top of the valence band. In this way, the valence band maxima of the oxides of La and Y are shifted down in energy, resulting in the increased electronic band gaps. For both $La_2Sn_2O_7$ and $Y_2Sn_2O_7$, the Sn 5d and O 2p states are dominant at the top of the valence band. The calculated partial charges further illustrate the electronic differences between the presence of Bi and Y/La in the Sn pyrochlore by showing an increase in effective oxidation state (and reduction in covalent character) from Bi → La → Y.

It is interesting to note that the asymmetry in the electron density of Bi is much weaker than that of Pb and Sn in similar distorted structures. Indeed, this is reflected in the energy differences between corresponding symmetric and distorted crystal structures. For $Bi_2Sn_2O_7$, there is a 0.2 eV difference between the symmetric and distorted phases, making the symmetric phase accessible at high temperatures where the available thermal energy can overcome the enhanced stability of the distorted structure. In contrast, for PbO there is a 0.4 eV difference between the distorted litharge and symmetric rocksalt lattices,[23] with a 0.9 eV difference for SnO[19] making the higher-energy symmetric structure thermodynamically inaccessible under standard conditions. This trend also exists in the relative stabilities of the competing oxides formed from group 14 and 15 metals. Sn is equally stable in both its higher and lower oxidation states, forming $Sn^{II}O$ and $Sn^{IV}O_2$, respectively. Pb exists as $Pb^{II}O$, and while $Pb^{IV}O_2$ is relatively stable, it is very susceptible to reduction and nonstoichiometry. For Bi, $Bi^{III}_2O_3$ is chemically stable, but the higher-oxidation-state oxide $Bi^{V}_2O_{10}$ is very hard to obtain under standard conditions. In each case, the increased binding energy of the metal s states effectively reduces the overlap with O 2p. Hence, formation of the higher-oxidation-state oxide, which requires the emptying of at least some of the low-energy metal s states, is more energetically costly on transition from Sn → Pb → Bi. Further demonstration of this competition is illustrated effectively when the metals are used as components in ternary oxide systems; i.e., in $Bi_2Sn_2O_7$ and Bi_{12}-

(45) Bader, R. F. W. *Acc. Chem. Res.* **1985**, *18*, 9.
(46) Henkelman, G.; Arnaldsson, A.; Jonsson, H. *Comput. Mater. Sci.* **2006**, *36*, 354.
(47) Godinho, K.; Walsh, A.; Watson, G. W., *unpublished.*

PbO_{20},[48] Bi adopts the lower oxidation state, while in $Sn_2Pb_2O_6$,[49] Pb adopts the lower oxidation state.

Conclusion

The electronic structure of the α- and γ-phases of bismuth stannate, $Bi_2Sn_2O_7$, and the thermodynamically stable phases of $La_2Sn_2O_7$ and $Y_2Sn_2O_7$ have been calculated using gradient-corrected DFT. Complete ionic position and cell relaxations were performed, and the resulting structures are in very good agreement with experiment. The calculated binding energies correctly predict α-$Bi_2Sn_2O_7$ as the stable phase of $Bi_2Sn_2O_7$.

Strong interactions occur between oxygen and both Sn and Bi in both phases of $Bi_2Sn_2O_7$. The compounds show covalent character with partial charges of approximately +2 and +2.5 for Bi and Sn, respectively. A mixture of Bi 6s and O 2p states is found to dominate the top of the valence band, while Sn 5s, O 2p, and Bi 6p states dominate the bottom of the conduction band; this is due to differences in the strength of the metal s interactions with O 2p. Differences in the electronic structure of α- and γ-$Bi_2Sn_2O_7$ come in the coupling of Bi 6p with high-energy O 2p and Bi 6s states at the top of the valence band. For α-$Bi_2Sn_2O_7$, this coupling leads to the formation of an asymmetric electronic density on Bi, which helps compensate for the lost oxygen coordination in the distorted structure. For γ-$Bi_2Sn_2O_7$, the symmetric coordination environment inhibits the coupling of Bi 6p at the top of the valence band, and the structure is less-favored energetically. Replacing Bi with Y or La in the Sn pyrochlores greatly reduces the covalent interactions with O 2p, with the metals making very little contribution to the valence band. In this way, no high-energy states are produced, and the band gap increases due to a reduction in the level of the valence-band maxima. The results provide a basis for understanding the origins of structural distortion in bulk $Bi_2Sn_2O_7$. To explain the catalytic and gas-sensing properties, it would be beneficial for future studies to focus on the relative surface stabilities, whether Sn, Bi, or O terminations are favored, and the formation of intrinsic defects which are abundant in the related transparent conducting oxide SnO_2.

Acknowledgment. We would like to acknowledge the HEA for a PRTLI (Cycle III) grant and thank David Scanlon for useful discussions. All calculations were performed on the IITAC cluster maintained by the TCHPC at the University of Dublin.

CM0714279

(48) Mazumdar, S. *Indian J. Phys., A* **1993**, *67*, 45.
(49) Badarau, M.; Michel, M. A. *Ann. Chim.* **1971**, *1971*, 109.